TG-FTIR study on co-combustion of bituminous coal semicoke and lignite

Ruidong Zhao[1] · Jianguang Qin[1] · Tianju Chen[1] · Jinhu Wu[1]

Abstract

The combustion behaviors and pollutants emission characteristics during co-combustion of bituminous coal semicoke and lignite were investigated by thermogravimetric analyzer coupled with Fourier transform infrared spectrometer (TG-FTIR). Results showed the addition of lignite could lower the ignition and burnout temperature and also enhance the comprehensive combustion performance of blends. High heating rate could improve the combustion intensity and corresponding combustion characteristic indexes. The activation energy analysis by distributed activation energy model (DAEM) and Ozawa–Flynn–Wall (OFW) methods at lignite blend ratio of 40% indicated its distribution was consistent with the combustion process of blends. An obvious activation energy jump occurred at conversion rate range of 0.4–0.55 due to the poor ignition performance of semicoke. The average activation energy obtained by DAEM and OFW methods was 101.69 kJ mol^{-1} and 109.12 kJ mol^{-1}, respectively. With the increase of lignite blend ratios, CO and CO_2 emission gradually decreased. Meanwhile, NO emission increased, while NO_2 and SO_2 emission ascended after an initial decline. Semicoke had certain suppression effect on NOx and SO_2 emission. The minimum NO_2 and SO_2 emission was obtained at lignite blend ratio of 20%.

Keywords Semicoke · Lignite · Co-combustion · TG-FTIR · Gaseous pollutants

Introduction

Pyrolysis has become one of the most efficient and clean technologies to realize cascade utilization of low rank coal, especially in China [1]. Semicoke is the solid product of low-rank coal pyrolysis process, and it is generally used in the chemical and metallurgical industry. But compared with its rapidly increasing production, the semicoke consumption in traditional industry is relatively limited [2]. As a result, large amount of semicoke piles up which causes great damage to the land, water and air and also the waste of resources. Due to the high calorific value and low pollution elements content, semicoke can be used as high grade and clean fuel. However, the volatile content in semicoke is very low and may result in the difficulty of ignition and burnout

✉ Ruidong Zhao
zhaord@qibebt.ac.cn

✉ Jinhu Wu
wujh@qibebt.ac.cn

1 Key Laboratory of Biofuels, Qingdao Institute of Bioenergy and Bioprocess Technology, Chinese Academy of Sciences, Qingdao 266101, China

[3]. Co-combustion with high volatile fuel is a feasible way to avoid these drawbacks [4]. In recent years, because of the gradual depletion and rising price of high-grade coal, lignite-fired power plants grow rapidly, especially near the lignite mines [5]. Lignite is one of the low rank coals and has high volatile content. Hence, co-combustion of semicoke with lignite can effectively improve the ignition and burnout performance of semicoke which is promising for its large-scale utilization in existing lignite-fired power plants.

The co-combustion of different coals and coal with biomass or sewage sludge has been widely studied [6–8]. By contrast, the studies on the co-combustion of coal and its semicoke are few. Hu et al. [9] studied the combustion characteristics of bituminous coal blended with semicoke by use of thermogravimetric analyzer (TGA) and drop tube furnace. The results showed semicoke blending could increase ignition and burnout temperatures and reduce NOx emission under certain conditions. Similar works were also conducted by Zhang et al. [10], and a linear regression model was established to predict the NO conversion during co-combustion. Yao et al. [11] found ignition temperature of semicoke blended bituminous coal in 21%O_2/79%CO_2 atmosphere was higher than that in air. With the increase of

O_2 concentration in oxy-fuel combustion, the co-combustion characteristics could be improved, but the activation energy gradually increased. Yuan et al. [12] pointed out in the co-combustion of lignite and semichar, the homogeneous ignition was dominant at low semichar fraction, while heterogeneous ignition was easier when the fraction of semichar was above 50%. Better burnout characteristics appeared in the region of 10–60% semichar fraction. Chen et al. [13] investigated the co-combustion characteristics of bituminous coal/char mixtures after reduction reaction with NO by a microfluidized bed analyzer and found the combustion reactivity of blends became worse and NO cumulative emission increased with the increase of char ratio. Ding et al. [14] studied the co-combustion characteristics of low-rank coal semicoke and municipal solid waste at different atmosphere. The results indicated the addition of municipal solid waste and higher oxygen concentration improved the co-combustion performance of blends and oxy-fuel atmosphere was conducive to semicoke burnout.

As listed above, there are fewer studies focused on the co-combustion of semicoke and lignite. In this research, the co-combustion behaviors of semicoke and lignite were investigated by use of TG-FTIR. The combustion, kinetics and gaseous pollutants emission characteristics during co-combustion were discussed in detail. The results will provide useful support for the large-scale utilization of semicoke.

Experimental

Samples

Semicoke was provided by Shaanxi Coal and Chemical Industry Group Co., Ltd (Shaanxi Province, China). It was the pyrolysis product of Shenmu bituminous coal. Lignite was collected from Naomaohu district (Xinjiang Province, China). Both the semicoke and lignite samples were prepared according to Chinese standard GB 474–2008 and pulverized to particle size of 75 μm. The proximate, ultimate, ash and

heating value analysis of the samples was conducted according to Chinese standard (GB/T 212–2008, DL/T 568–2013, DL/T 1037–2016 and GB/T 213–2008, respectively), and the results are shown in Tables 1 and 2. They were directly mixed according to the lignite blend ratios (the mass fraction of lignite in the blends). The lignite blend ratios were 0, 20%, 40%, 60%, 80% and 100%, respectively.

TG-FTIR apparatus and methods

TG-FTIR experiments were carried out on a METTLER-TOLEDO TGA 2 thermogravimetric analyzer coupled with a BRUKER TENSOR II Fourier transform infrared spectrometer. In each TG experiment, about 10 mg samples was used and then heated to 1000 °C under air atmosphere of 60 mL min^{-1}. The heating rate was 10, 20 and 30 °C min^{-1}, respectively. The gaseous products of TG experiments were directly sent to the FTIR through a heated transfer line with the temperature of 250 °C. The spectrum range of FTIR was 600–4000 cm^{-1} with a resolution of 4 cm^{-1} and scanning times of 8. The TGA experiments were repeated twice to ensure the reproducibility, and the results showed good repeatability.

Data analysis methods

Characteristic parameters were defined to evaluate the co-combustion performance of semicoke and lignite. Temperature when the sample began to burn was ignition temperature (T_i) and could be determined by TG-DTG tangent method [15, 16]. Burnout temperature (T_f) was defined as the temperature when the mass loss reached 98% of the total mass loss [17]. The comprehensive combustion index S, ignition index D_i and burnout index D_f were determined by the equation as follows [18, 19]:

$$S = \frac{DTG_m DTG_a}{T_i^2 T_f} \tag{1}$$

Table 1 Proximate and ultimate analysis of samples (air dry basis)

Samples	Proximate analysis/mass%				Ultimate analysis/mass%					LHV
	M	V	A	FC*	C	H	N	S	O*	MJ/kg
Semicoke	10.20	7.96	9.87	71.97	72.45	1.29	0.87	0.38	4.94	23.04
Lignite	18.68	38.10	5.31	37.91	57.33	3.88	0.85	0.38	13.57	22.06

M moisture, *V* volatile, *A* ash, *FC* fixed carbon, *LHV* lower heating value, * by difference

Table 2 Ash analysis of samples (mass%)

Samples	SiO$_2$	Al$_2$O$_3$	Fe$_2$O$_3$	CaO	MgO	K$_2$O	Na$_2$O
Semicoke ash	35.93	1.48	1.15	34.66	3.77	13.39	0.65
Lignite ash	25.67	12.72	15.46	25.50	3.53	0.26	4.24

$$D_i = \frac{DTG_m}{t_i t_m} \qquad (2)$$

$$D_f = \frac{DTG_m}{\Delta t_{1/2} t_m t_f} \qquad (3)$$

where DTG_m was the maximum mass loss rate, DTG_a was the average mass loss rate (from ignition to burnout). t_i, t_m and t_f were the corresponding time of ignition, maximum mass loss rate and burnout, respectively. $\Delta t_{1/2}$ was the time span of DTG/ $DTG_m = 0.5$ in the both sides of DTG curve peak.

CO_2, CO, NO, NO_2 and SO_2 were identified by their characteristic bands in infrared absorbance spectra and used to evaluate the gaseous pollutants emission characteristics during co-combustion. The typical infrared characteristic peaks of CO_2, CO, NO, NO_2, and SO_2 were 2360, 2176, 1520, 1762 and 1342 cm^{-1}, respectively [20–22].

Results and discussion

Co-combustion characteristics of semicoke and lignite

Influence of lignite blend ratios

Figure 1 shows the TG and DTG curves as a function of temperature under different lignite blend ratios (heating rate is 20 °C min^{-1}). The corresponding parameters of TG and DTG curves are shown in Table 3. From Fig. 1, both the semicoke and lignite have three mass loss stages. The moisture removal stage at the temperature lower than 200 °C and the residue decomposition stage after burnout are not further discussed in the present paper. The main mass loss stage of semicoke is in the temperature range of 410–750 °C with a DTG peak at 619 °C while that of lignite is in the temperature range of 217–550 °C with a DTG peak at 389 °C.

When lignite blend ratios are 20–60%, the combustion process of blends has two main mass loss stages. With the increase of lignite blend ratios, the first DTG peak increases, while the second DTG peak decreases. Both the
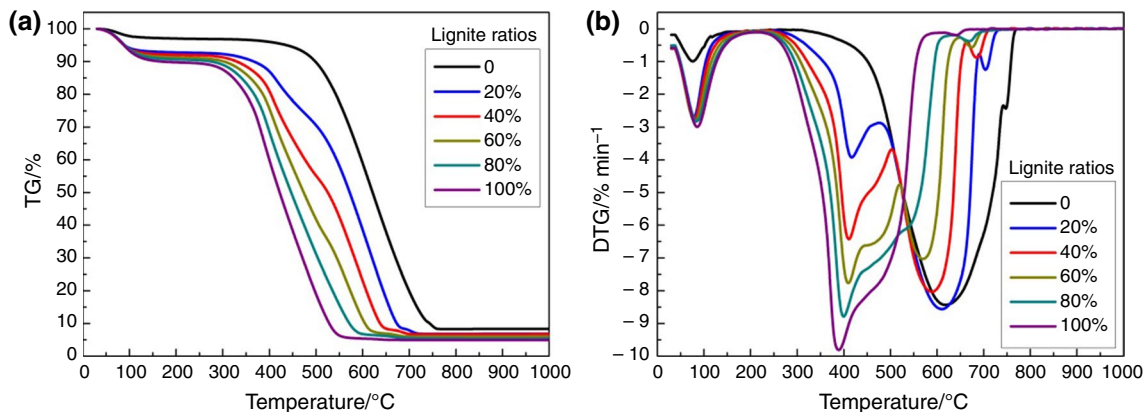

Fig. 1 TG (**a**) and DTG (**b**) curves at different lignite blend ratios (heating rate 20 °C min^{-1})

Table 3 TG and DTG curves parameters at different lignite blend ratios and heating rates

Lignite ratios	β/°C min^{-1}	Stage 1		Stage 2		T_m/°C	DTG_m/% min^{-1}	DTG_a/% min^{-1}
		Interval/°C	Mass loss/%	Interval/°C	Mass loss/%			
0	20	–	–	410–750	86.6	619.0	8.43	6.67
20%	20	248–476	18.4	476–685	65.7	610.7	8.56	6.27
40%	20	236–502	37.1	502–651	46.4	589.0	8.03	5.57
60%	20	221–520	54.5	520–620	28.9	409.7	7.76	5.97
80%	20	216–585	82.8	–	–	400.0	8.78	6.34
100%	20	217–550	83.3	–	–	389.0	9.81	7.28
40%	10	222–475	36.9	475–596	47.2	559.0	6.36	3.35
40%	30	237–455	21.6	455–706	61.8	604.5	8.74	7.05

corresponding temperature of DTG peaks decreases and TG curves integrally shifts to the lower temperature zone which means the combustion of blends is ahead of time. It can be attributed to the increasing volatile content of blends after addition of lignite. The heat release in volatile combustion process will preheat semicoke and promote the combustion of semicoke in advance [19]. When lignite blend ratio is 80%, the DTG curve only has one mass loss peak which is similar to lignite. It also confirms that the combustion period of semicoke is greatly moved up and has been mixed with lignite combustion stage.

Table 4 shows the co-combustion characteristic parameters at different lignite blend ratios. Obviously, both T_i and T_f gradually decrease with the increasing lignite blend ratios. When lignite blend ratio increases to 80%, T_i and T_f of the blends are 159 °C and 153 °C lower than that of semicoke, respectively. Accordingly, D_i increases from 1.2×10^{-2} to 2.97×10^{-2}, D_f increases 0.75×10^{-3} to 1.65×10^{-3} and S increases from 2.93×10^{-7} to 7.72×10^{-7}. It means ignition, burnout and comprehensive combustion performance of blends has been greatly enhanced with the addition of lignite.

Influence of heating rates

Figure 2 shows the TG and DTG curves of blends (lignite blend ratio is 40%) at different heating rates (10, 20 and 30 °C min^{-1}). The corresponding combustion characteristic parameters are also listed in Table 3 and Table 4. With the increase of heating rates, TG and DTG curves move to the higher-temperature zone and the main mass loss occurs in wider temperature ranges. Besides, all of the T_i, T_m and T_f gradually increase which indicates that the combustion is postponed. It can be attributed to the hysteresis between the heating temperature of TGA and the actual temperature of fuel particles [23]. However, the heat transfer intensity from the surface of fuel particles to the center can also be enhanced at high heating rates [24]. Therefore, the maximum and average mass loss rates rapidly increase with the increasing heating rates which means the combustion intensity of blends is improved. As a result, the S, D_i and D_f of blends also gradually increase.

Kinetic analysis

Two model-free methods, the distributed activation energy model (DAEM) method and Ozawa–Flynn–Wall (OFW)

Table 4 Co-combustion characteristic parameters at different lignite blend ratios and heating rates

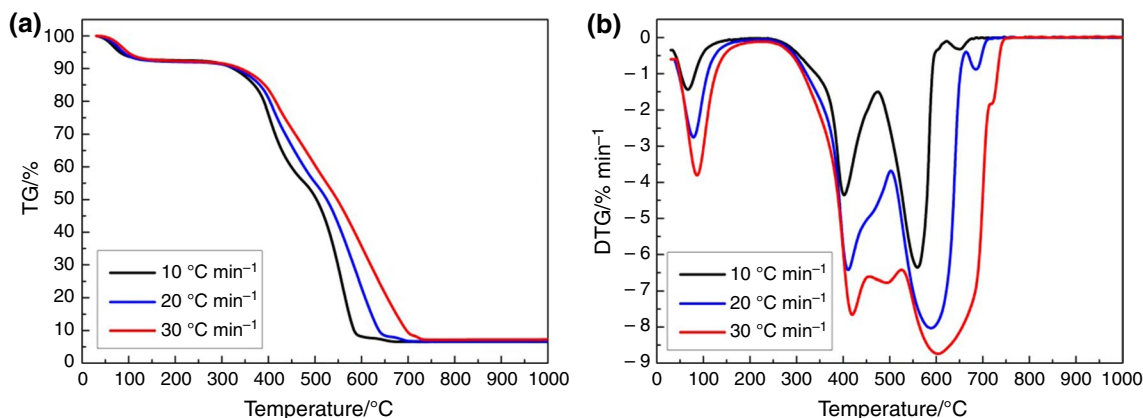| Lignite ratios	β/°C min^{-1}	T_i/°C	T_f/°C	$S \times 10^{-7}$/ min^{-2}°C^{-3}	$D_i \times 10^{-2}$/min^{-3}	$D_f \times 10^{-3}$/min^{-3}
0	20	508.6	742.7	2.93	1.20	0.75
20%	20	471.5	682.0	3.54	1.34	1.14
40%	20	366.7	647.7	5.14	1.71	1.48
60%	20	360.4	617.3	5.78	2.47	1.55
80%	20	349.7	589.7	7.72	2.97	1.65
100%	20	337.3	545.0	11.52	3.56	2.39
40%	10	362.2	593.5	2.74	0.36	0.29
40%	30	369.0	702.5	6.44	4.04	1.97

Fig. 2 TG (**a**) and DTG (**b**) curves at different heating rates (lignite blend ratio is 40%)

method were used to evaluate the change of activation energy during co-combustion process. A typical condition with lignite blend ratio of 40% and heating rate of 10, 20 and 30 °C min^{-1} was selected for kinetic analysis. DAEM method determines the kinetic parameters by assuming that an infinite number of first-order parallel reactions occur simultaneously and the activation energy of these reactions are described as a Gaussian distribution [25]. It is widely used in the kinetic study of solid fuels thermochemical conversion process and has been proven to be effective [26]. The classical DAEM kinetic equation simplified by Miura–Maki method is shown in Eq. (4) [27, 28]. The OFW kinetic equation simplified by Doyle's approximation is shown in Eq. (5) [29, 30].

$$\ln\left[\frac{\beta}{T^2}\right] = -\frac{Ea}{R}\frac{1}{T} + \ln\left[\frac{AR}{Ea}\right] + 0.6075 \tag{4}$$

$$\ln\beta = -1.052\frac{Ea}{R}\frac{1}{T} + C \tag{5}$$

where, x is conversion rate. Ea, A, β and R are the activation energy, pre-exponential factor, heating rates and universal gas constant, respectively. For a certain value of x, Ea can be obtained from the slope of the fitting straight line of ln β/T^2 or ln β versus $1/T$ at different heating rates. Then, the change of Ea can be obtained by the similar calculation at different values of x.

Figure 3a shows the change of Ea determined by DAEM and OFW methods at different x (0.15–0.95). The detailed data can be found in Table 5. All of the coefficients (R^2) obtained by DAEM and OFW methods are greater than 0.93 and 0.95, respectively. Moreover, the values and change tendency of Ea obtained by the two methods are close to each other which show good accuracy. From Fig. 3a, the change of activation energy can be divided

into three stages. In the first stage (conversion rate range of 0.15–0.40), activation energy rapidly decreases. When volatile is released and begins to burn (the corresponding conversion rate of volatile ignition is around 0.15), the released heat and increased porosity enhance reactions between oxygen and the blends which reduces the activation energy [31, 32]. For the second stage (conversion rate range of 0.40–0.55), the initial temperature is 437.7, 465.1 and 489.2 °C, while the end temperature is 508.2, 530.3 and 552.0 °C, respectively (depending on the heating rates). Compared with the DTG curves in Fig. 2b, it is just the transition stage from lignite combustion to semicoke combustion. Due to the gradual burnout of volatile and the difficulty of semicoke ignition, the activation energy begins to increase. The third stage (conversion rate range of 0.55–0.95) is the combustion of semicoke. Though fixed carbon combustion is difficult and has large activation energy, once it is ignited, its combustion is violent and the activation energy will drop rapidly even lower than volatile combustion [33]. The average activation energy obtained by DAEM method and OFW method in the whole co-combustion process is 101.69 kJ mol^{-1} and 109.12 kJ mol^{-1}, respectively.

In order to further verify the reliability of DAEM method, the conversion curves of x versus T are re-calculated through Eq. (4) and obtained Ea and A by DAEM method. The comparison of calculated and experimental conversion curves of x versus T at the different heating rates is shown in Fig. 3b. From Fig. 3b, the calculated conversion curves are generally in good agreement with the experimental values. A tiny difference appears at the late period of conversion due to the slightly declining accuracy of kinetic analysis. The Pearson correlation coefficients of calculated and experimental results are greater than 0.99, indicating that the kinetic parameters obtained by DAEM method are reliable.
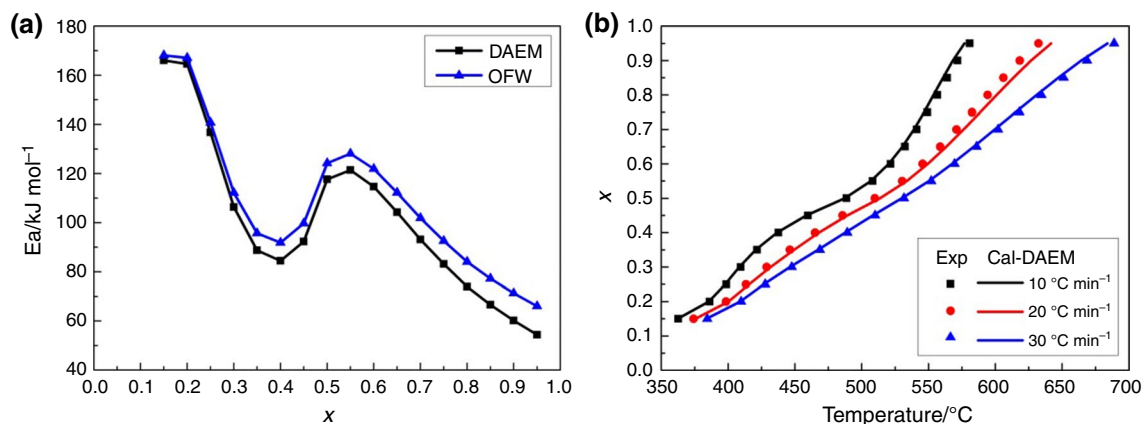

Fig. 3 Ea versus x (**a**) and experimental and DAEM calculated x versus T curves (**b**)

Table 5 Kinetic parameters determined by DAEM and OFW methods

x	DAEM method				OFW method			
	Slope	Intercept	R^2	Ea/kJ mol^{-1}	Slope	Intercept	R^2	Ea/kJ mol^{-1}
0.15	− 19,974.5	36.35	0.9746	166.07	− 21,267.4	35.78	0.9777	168.08
0.20	− 19,795.5	20.84	0.9709	164.58	− 21,137.2	34.39	0.9746	167.05
0.25	− 16,449.9	19.38	0.9593	136.76	− 17,822.2	28.87	0.9654	140.85
0.30	− 12,793.9	13.81	0.9612	106.37	− 14,196.4	23.14	0.9688	112.19
0.35	− 10,672.0	8.03	0.9716	88.73	− 12,107.0	19.76	0.9784	95.68
0.40	− 10,150.9	4.60	0.9768	84.39	− 11,622.1	18.68	0.9827	91.85
0.45	− 11,101.1	3.48	0.9669	92.29	− 12,615.5	19.55	0.9748	99.70
0.50	− 14,155.3	4.29	0.9510	117.69	− 15,721.0	22.98	0.9605	124.24
0.55	− 14,610.3	7.66	0.9589	121.47	− 16,215.7	23.10	0.9669	128.15
0.60	− 13,792.4	7.72	0.9555	114.67	− 15,428.7	21.75	0.9647	121.93
0.65	− 12,537.8	6.34	0.9480	104.24	− 14,201.2	19.98	0.9598	112.23
0.70	− 11,203.5	4.53	0.9459	93.15	− 12,891.4	18.18	0.9596	101.88
0.75	− 10,001.5	2.70	0.9429	83.15	− 11,713.0	16.59	0.9590	92.57
0.80	− 8897.5	1.09	0.9411	73.97	− 10,632.4	15.16	0.9596	84.03
0.85	− 8012.2	− 0.37	0.9389	66.61	− 9770.5	14.02	0.9599	77.22
0.90	− 7240.5	− 1.54	0.9365	60.20	− 9023.5	13.03	0.9603	71.31
0.95	− 6546.4	− 2.56	0.9314	54.43	− 8357.9	12.13	0.9594	66.05
average	–	–	–	101.69	–	–	–	109.12
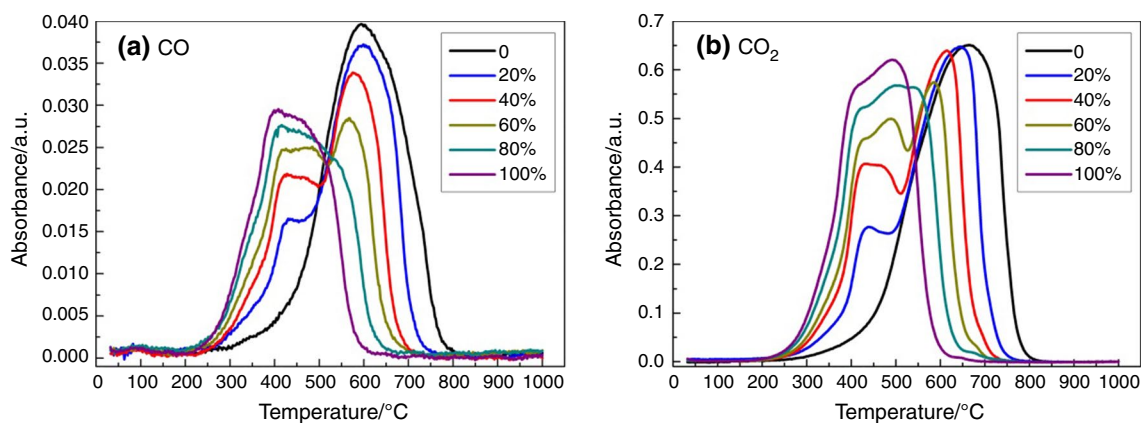
Fig. 4 CO (**a**) and CO$_2$ (**b**) emission curves at different lignite blend ratios

Gaseous pollutants emission characteristics

CO and CO$_2$ emission

Figure 4 shows the CO and CO$_2$ emission curves at different lignite blend ratios. The corresponding integral values are shown in Table 6. Because the samples mass used in TG experiments are not exactly the same, the values listed in Table 6 are the total integral areas divided by the sample mass. The CO and CO$_2$ emission temperature of semicoke is around 450–750 °C, while that of lignite is around 350–600 °C. It is consistent with the main mass loss stages of semicoke and lignite. The CO and CO$_2$ emission curves of blends have two absorption peaks. As the increase of lignite

Table 6 Integral values of CO, CO$_2$, NO, NO$_2$ and SO$_2$ at different lignite blend ratios (per mg of blends)

Lignite ratios	CO	CO$_2$	NO	NO$_2$	SO$_2$
0	0.8360	13.6229	0.2462	0.3368	0.2561
20%	0.8180	13.3198	0.2472	0.3071	0.2558
40%	0.7169	12.9180	0.2511	0.3386	0.2762
60%	0.6990	12.6085	0.2534	0.3598	0.2958
80%	0.6260	12.1207	0.2582	0.4095	0.3132
100%	0.5656	11.2581	0.2621	0.4285	0.3405

blend ratio, the first absorption peak corresponding to lignite combustion ascends, while the second absorption peak generated by semicoke combustion descends. From Table 6, it can be found that both CO and CO_2 emission values gradually decrease with the increase of lignite blend ratios. It indicates CO and CO_2 emission during co-combustion is mainly determined by the carbon content in the blends.

NOx emission

Figure 5 shows the NOx emission curves changing with temperature at different lignite blend ratios. As shown in Fig. 5, NO and NO_2 emission tendency is close to CO and CO_2. The nitrogen in semicoke tends to be released at high temperature, while the nitrogen release temperature of lignite is low. The NOx emission curves of blends locate between semicoke and lignite. An extra tiny peak appears at around 100 °C which is mainly the interference of H_2O. From the NOx integral values shown in Table 6, with the increasing lignite blend ratio, NO emission gradually increases, whereas NO_2 emission rises after an initial decrease. NO

and NO_2 emission of semicoke is 0.2462 and 0.3368, respectively, while that of lignite is 0.2621 and 0.4285. Obviously, the growth of NO_2 emission is larger than NO emission. It indicates NO_2 is easier to be formed in lignite combustion. Lignite is the geologically youngest coal and has high oxygen containing groups such as $-HO_2$ and $-OH$. Hence, the formation reaction of NO_2 shown in Eq. (6) and Eq. (7) will be more intense [34].

$$NO + HO_2 \rightarrow NO_2 + OH \tag{6}$$

$$NO + OH \rightarrow NO_2 + H \tag{7}$$

In order to further evaluate the interaction between semicoke and lignite on NOx emission, the comparison of experimental and calculated NOx integral areas is shown in Fig. 6. The calculated NOx integral area is defined in Eq. (8).

$$IA_{calculation} = \alpha_{semicoke}IA_{semicoke} + \alpha_{lignite}IA_{lignite} \tag{8}$$
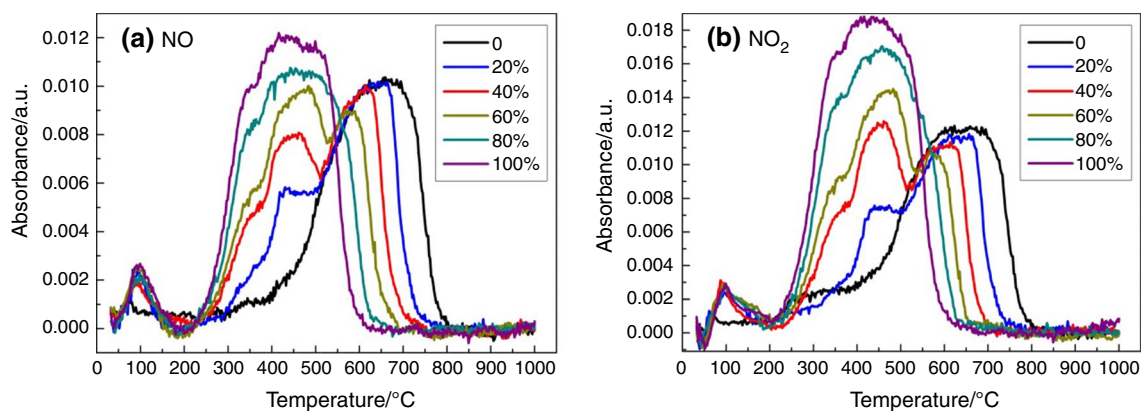

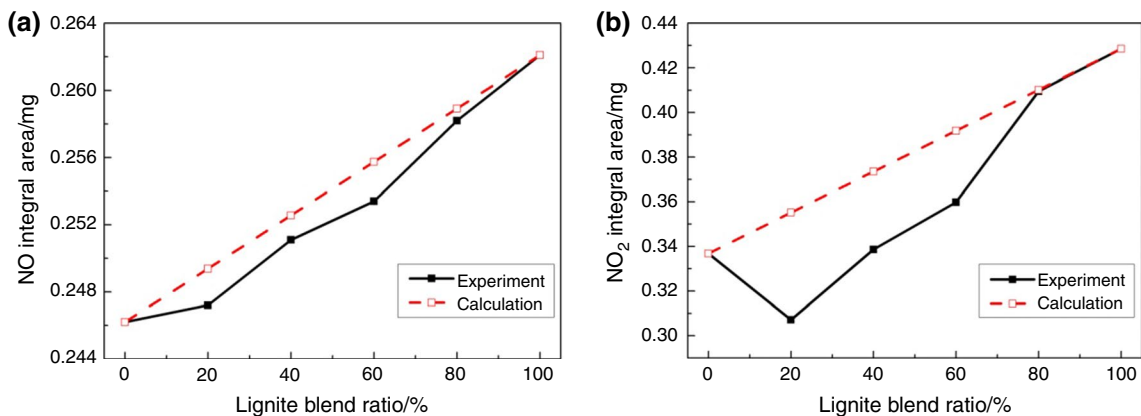Fig. 5 NO (**a**) and NO_2 (**b**) emission curves at different lignite blend ratios

Fig. 6 Experimental and calculated NO (**a**) and NO_2 (**b**) integral area at different lignite blend ratios
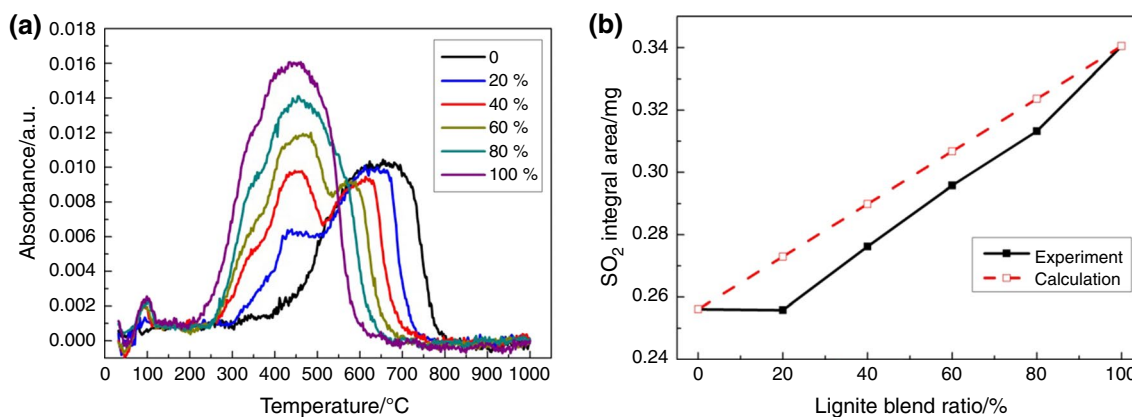
Fig. 7 SO_2 emission curves (**a**) and integral area comparison (**b**) at different lignite blend ratios

$IA_{semicoke}$ and $IA_{lignite}$ are the integral area of individual semicoke and lignite, respectively, and $\alpha_{semicoke}$ and $\alpha_{lignite}$ are their corresponding blend ratios.

From Fig. 6, all of the experimental NOx values are lower than calculated values which indicate suppression effect on NOx emission exists in co-combustion. The differences between calculated and experimental values will shrink with the increase of lignite blend ratios, especially for the NO_2 emission. It implies semicoke is beneficial to reduce the NOx emission in the co-combustion. The literature shows coal char is effective on NOx reduction by the heterogeneous reaction between NO and char [35]. Semicoke has higher char content and therefore can better suppress the NOx emission. Besides, from Table 6, more CO will be produced in semicoke combustion. As a result, the homogeneous reduction reaction between CO and NOx will be enhanced [36]. In addition, the abundant metallic components (Ca, Fe, Na and K) in ash (shown in Table 2) also have catalytic effect on the reduction reaction of NOx with coal char and CO which further reduce the NOx emission [37, 38]. When lignite blend ratio is 20%, the suppression effect on NO_2 is even stronger than the motivating influence of added lignite which results in the minimum NO_2 emission.

SO$_2$ emission

The emission curves of SO_2 varying with temperature are shown in Fig. 7a. The peak temperature of SO_2 release curve for semicoke is 645 °C which is much higher than that of lignite (461 °C). With the increase of lignite blend ratios, SO_2 tends to be released at low temperature. From Table 6, the total SO_2 emission for semicoke is 0.2561 which is obviously lower than lignite (0.3405). However, as shown in Table 1, the sulfur content in semicoke is the same as lignite. It indicates sulfur in semicoke is difficult to release in co-combustion process. This can be interpreted from two factors. Firstly, semicoke is the pyrolysis product of

bituminous coal and incombustible sulfate sulfur is enriched in semicoke [39]. Secondly, from Table 1 and Table 2, semicoke has higher alkaline and alkali metal content in the ash. Therefore, self-retention of sulfur by semicoke ash is more significant [40]. From Table 6, it can be also obtained that the total SO_2 emission increases with the increasing lignite blend ratios except for a slight decline at 20%.

Figure 7b shows the comparison of calculated and experimental SO_2 emission. The calculation method is the same as NOx emission. From Fig. 7b, the calculated SO_2 emission is always higher than experimental values. It means inhibiting effect on SO_2 emission also exists in the co-combustion. As mentioned above, semicoke has well self-desulfurization capability which is also effective in the combustion process of blends. The more semicoke the blends contain, the stronger the SO_2 inhibiting effect is. This can be confirmed by the narrowing gap between calculated and experimental values with the increase of lignite blend ratio. As a result, the minimum SO_2 emission is obtained at lignite blend ratio of 20%.

Conclusions

Co-combustion behaviors of semicoke and lignite were investigated by TG-FTIR. The results show the combustion characteristics of semicoke were greatly improved and the gaseous pollutants could also be reduced with the addition of lignite. The main conclusions are summarized as follows:

(1) The addition of lignite can lower the ignition and burnout temperature and improve ignition index D_i, burnout index D_f and comprehensive combustion index S. The D_i, D_f and S increase from 1.2×10^{-2} to 2.97×10^{-2}, 0.75×10^{-3} to 1.65×10^{-3} and 0.91×10^{-7} to 1.66×10^{-7}, respectively, when lignite blend ratio increases to 80%. High heating rates can improve the combustion

intensity and corresponding combustion characteristic indexes.

(2) The activation energy distribution determined by DAEM and OFW methods is consistent. An obvious activation energy jump occurs at conversion rate range of 0.4–0.55 because of the poor ignition performance of semicoke. The average activation energy obtained by DAEM and OFW methods is 101.69 kJ mol^{-1} and 109.12 kJ mol^{-1}, respectively.

(3) With the increase of lignite blend ratio, the CO and CO_2 emission gradually decrease. Simultaneously, the NO emission increases, while the NO_2 and SO_2 emission rises after an initial decrease. Semicoke has certain suppression effect on NOx and SO_2 emission. The minimum NO_2 and SO_2 emission is obtained at lignite blend ratio of 20%.

Compliance with ethical standards

Conflict of interest The authors declare that they have no conflict of interest.

References

1. Xue FF, Li D, Guo YT, Zhang XP, Zhou QC, Ma BQ. Technical progress and prospect of low lank coal pyrolysis in China. Energy Technol. 2017;5(11):1897–907.
2. Wang CA, Feng QQ, Lv Q, Zhao L, Du YB, Wang PQ, Zhang JW, Che DF. Numerical investigation on co-firing characteristics of semi-coke and lean coal in a 600 MW supercritical wall-fired boiler. Appl Sci. 2019;9:889.
3. Zhu SJ, Lyu QG, Zhu JG, Wu HX, Wu GL. effect of air distribution on NOx emissions of pulverized coal and char combustion preheated by a circulating fluidized bed. Energy Fuels. 2018;32:7909–15.
4. Wang PQ, Wang CA, Du YB, Feng QQ, Wang ZC, Yao W, Liu JL, Zhang JP, Che DF. Experiments and simulation on co-combustion of semicoke and coal in a full-scale tangentially fired utility boiler. Energy Fuels. 2019;33:3012–27.
5. Li ZX, Miao ZQ, Shen XS. Combined effects of water content and primary air volume on performance of lignite-fired boiler. Fuel. 2019;244:580–91.
6. Dios M, Souto JA, Casares JJ. Experimental development of CO_2, SO_2 and NOx emission factors for mixed lignite and sub-bituminous coal-fired power plant. Energy. 2013;53:40–51.
7. Mortari DA, Torquato LDM, Crespi MS, Crnkovic PM. Co-firing of blends of sugarcane bagasse and coal. J Therm Anal Calorim. 2018;132:1333–45.
8. Niu SB, Chen MQ, Li Y, Song JJ. Co-combustion characteristics of municipal sewage sludge and bituminous coal. J Therm Anal Calorim. 2018;131:1821–34.
9. Hu LL, Zhang Y, Chen DG, Fang JG, Zhang M, Wu YX, Zhang H, Li ZS, Lyu JF. Experimental study on the combustion and NOx emission characteristics of a bituminous coal blended with semi-coke. Appl Therm Eng. 2019;160:113993.
10. Zhang JP, Jia XW, Wang CA, Zhao N, Wang PQ, Che DF. Experimental investigation on combustion and NO formation characteristics of semi-coke and bituminous coal blends. Fuel. 2019;247:87–96.
11. Yao HF, He BS, Ding GC, Tong WX, Kuang YC. Thermogravimetric analyses of oxy-fuel co-combustion of semi-coke and bituminous coal. Appl Therm Eng. 2019;156:708–21.
12. Yuan Y, Li SQ, Yao Q. Experimental and numerical analyses on ignition and burnout characteristic of low-rank lignite and semi-char blends. In: Yue G, Li S, editors. Clean Coal Technology and Sustainable Development. ISCC 2015. Springer: Berlin; 2016. p. 69–74.
13. Chen L, Qiu PH, Sun SZ, Liu L, Zhao YJ, Sun R. NO reduction and emission characteristics of coal/char mixtures in a micro-fluidized bed reaction analyzer. Energy Fuels. 2019;33:276–86.
14. Ding GC, He BS, Yao HF, Cao Y, Su LB, Duan ZP. Co-combustion behaviors of municipal solid waste and low-rank coal semicoke in air or oxygen/carbon dioxide atmospheres. J Therm Anal Calorim. 2019. https://doi.org/10.1007/s10973-019-09170-z.
15. Zhang KH, Zhang K, Cao Y, Pan WP. Co-combustion characteristics and blending optimization of tobacco stem and high-sulfur bituminous coal based on thermogravimetric and mass spectrometry analyses. Biores Technol. 2013;131:325–32.
16. Niu SL, Han KH, Lu CM. Characteristic of coal combustion in oxygen/carbon dioxide atmosphere and nitric oxide release during this process. Energy Conv Manag. 2011;52:532–7.
17. Lin YS, Ma XQ, Ning XX, Yu ZS. TGA-FTIR analysis of co-combustion characteristics of paper sludge and oil-palm solid wastes. Energy Convers Manag. 2015;89:727–34.
18. Wang Q, Wang GW, Zhang JL, Wang HY. Thermal and kinetic behaviors of pyrolytic carbon black and gas coal in co-combustion. J Therm Anal Calorim. 2019;137:193–204.
19. Zhang YY, Guo YX, Cheng FQ, Yan KZ, Cao Y. Investigation of combustion characteristics and kinetics of coal gangue with different feedstock properties by thermogravimetric analysis. Thermochim Acta. 2015;614:137–48.
20. Wang CP, Wu YJ, Liu Q, Yang HR, Wang FY. Analysis of the behaviour of pollutant gas emissions during wheat straw/coal cofiring by TG-FTIR. Fuel Process Technol. 2011;92:1037–41.
21. Tian LN, Yang W, Chen ZH, Wang XH, Yang HP. Sulfur behavior during coal combustion in oxy-fuel circulating fluidized bed condition by using TG-FTIR. J Energy Inst. 2016;89:264–70.
22. Kok MV, Varfolomeev MA, Nurgaliev DK. Crude oil characterization using TGA-DTA, TGA-FTIR and TGA-MS techniques. J Petrol Sci Eng. 2017;154:537–42.

23. Li JP, Hu JQ, Wang T, Gan JH, Xie JP, Shui YH, Liu JX, Xue YJ. Thermogravimetric analysis of the co-combustion of residual petrochemical sludge and municipal sewage sludge. Thermochim Acta. 2019;673:60–7.

24. Zhao RD, Qin JG, Chen TJ, Wang LL, Wu JH. Experimental study on co-combustion of low rank coal semicoke and oil sludge by TG-FTIR. Waste Manag. 2020;116:91–9.

25. Zhang JZ, Chen TJ, Wu JL, Wu JH. Multi-Gaussian-DAEM-reaction model for thermal decompositions of cellulose, hemicellulose and lignin: Comparison of N_2 and CO_2 atmosphere. Biores Technol. 2014;166:87–95.

26. Huang YW, Chen MQ, Li Y. An innovative evaluation method for kinetic parameters in distributed activation energy model and its application in thermochemical process of solid fuels. Thermochim Acta. 2017;655:42–51.

27. Miura K, Maki T. A simple method for estimating f(e) and k0(e) in the distributed activation energy model. Energy Fuels. 1998;12:864–9.

28. Liu GR, Song HJ, Wu JH. Thermogravimetric study and kinetic analysis of dried industrial sludge pyrolysis. Waste Manag. 2015;41:128–33.

29. Yuan CD, Varfolomeev MA, Emelianov DA, Eskin AA, Nagrimanov RN, Kok MV, Afanasiev IS, Fedorchenko GD, Kopylova EV. Oxidation behavior of light crude oil and its SARA fractions characterized by TG and DSC techniques: differences and connections. Energy Fuels. 2018;32:801–8.

30. Varfolomeev MA, Nagrimanov RN, Galukhin AV, Vakhin AV, Solomonov BN, Nurgaliev DK, Kok MV. Contribution of thermal analysis and kinetics of Siberian and Tatarstan regions crude oils for in situ combustion process. J Therm Anal Calorim. 2015;122:1375–84.

31. Tas S, Yurum Y. Co-firing of biomass with coals: Part 2 Thermogravimetric kinetic analysis of co-combustion of fir (Abies bornmulleriana) wood with Beypazari lignite. J Therm Anal Calorim. 2012; 107:293–8.

32. Kok MV, Varfolomeev MA, Nurgaliev DK. Low-temperature oxidation reactions of crude oils using TGA-DSC techniques. J Therm Anal Calorim. 2020;141:775–81.

33. Zhou ZJ, Hu X, You Z, Wang ZH, Zhou JH, Cen KF. Oxy-fuel combustion characteristics and kinetic parameters of lignite coal from thermo-gravimetric data. Thermochim Acta. 2013;553:54–9.

34. Zhang YY, Ge XL, Liu LL, Wang XD, Zhang ZT. Fuel nitrogen conversion and release of nitrogen oxides during coal gangue calcination. Environ Sci Pollut R. 2015;22:7139–46.

35. Zhao K, Glarborg P, Jensen AD. NO reduction over biomass and coal char during simultaneous combustion. Energy Fuels. 2013;27:7817–26.

36. Shao LM, Fan SS, Zhang H, Yao QS, He PJ. SO_2 and NOx emissions from sludge combustion in a CO_2/O_2 atmosphere. Fuel. 2013;109:178–83.

37. Wang CA, Wang PQ, Du YB, Che DF. Experimental study on effects of combustion atmosphere and coal char on NO_2 reduction under oxy-fuel condition. J Energy Inst. 2019;92:1023–33.

38. Zhao ZB, Qiu JH, Li W, Chen HK, Li BQ. Influence of mineral matter in coal on decomposition of NO over coal chars and emission of NO during char combustion. Fuel. 2003;82:949–57.

39. Hou JL, Ma Y, Li SY, Shi J, He L, Li J. Transformation of sulfur and nitrogen during Shenmu coal pyrolysis. Fuel. 2018;231:134–44.

40. Lasek JA, Kazalski K. Sulfur self-retention during cocombustion of fossil fuels with biomass. Energy Fuels. 2014;28:2780–5.